Proceeding of the 9th International Symposium on Advanced Materials and Nanotechnology
(iSAMN2025), October 29-30, 2025

Enhancing Microstrip Patch Antenna Performance via Magnesium Tailoring of Ni-Zn Ferrites Structure

Nurul Ainaa Najihah **Busra**[1], Rodziah **Nazlan**[1*], Mohamad Ashry **Jusoh**[1]

[1] Faculty of Industrial Sciences and Technology,
Universiti Malaysia Pahang Al-Sultan Abdullah
Lebuh Persiaran Tun Khalil Yaakob 26300, Kuantan,
Pahang, Malaysia

*Corresponding author's phone: +609-4315627
E-mail: rodziah@umpsa.edu.my

Received: 28 October 2025; Accepted: 8 January 2026

ABSTRACT

Microstrip patch antennas (MPAs) are favored for their compactness and ease of integration, especially in wireless communication. Incorporating nickel zinc ferrites (NZF) as the radiating patch enhances the MPA performance by improving both bandwidth and return loss. However, optimizing the NZF properties is challenging, particularly through the introduction of Mg dopants, which can further enhance the performance of MPAs. Mg-NZF with Mg = 0.0 to 0.6 concentrations were synthesized using the mechanochemical technique. The effect of Mg variations on the NZF was characterized by their structural, microstructural and magnetic properties. The performance of the Mg-NZF as a radiating patch in MPA was evaluated through return loss and bandwidth measurement in the X-band frequency. XRD analysis confirms a single-phase spinel structure regardless of Mg concentrations, with a slight lattice parameter ranging from 8.3818 to 8.4010 Å attributed to Mg incorporation. Two main bands near 569.42 cm^{-1} and 425.66 cm^{-1} correspond to intrinsic vibrations of tetrahedral and octahedral Fe^{3+}–O^{2-} complexes. EM measurements show that MPA with Mg = 0.4 achieved the highest negative return loss of -37.98 dB at a resonant frequency of 7.95 GHz and a bandwidth of 1.12 GHz. Mg substitution improved the saturation magnetization (62.07 emu/g at $x = 0.4$), which enhanced impedance matching and radiation efficiency, leading to the highest return loss (-37.98 dB) and bandwidth (BW) (1.12 GHz) at 7.95 GHz. This increase in M_s correlates with improved superexchange interactions between magnetic moments. The combination of NZF and Mg leads to significant improvements in the microstructure and magnetic properties, facilitating better tuning and efficiency in the MPA performance.

Keywords— microstrip patch antenna, nickel zinc ferrites, magnesium dopant, magnetic properties, return loss optimization

1.0 INTRODUCTION

Undoubtedly, one of the most significant technologies nowadays is wireless communication technology because it enables communication without physical cables, allowing people to connect regardless of location. In addition, it also offers lower infrastructure costs and integrates a broad range of services and applications to meet the needs of users [1]. The rapid development of wireless communication technologies in the last decade has led to a new age of connectivity, driven largely by the advancements in 5G network. Antenna plays a central role as a critical interface between radar and wireless communication systems and the external environment. It transmits and receives radio frequency signals across diverse applications without noticeable interruptions or disruptions [2]. In order to accommodate the latest and most advanced technology, several electrical and microwave equipment are being updated daily in terms of both model and features. The evolution of wireless device models and trends, as well as the modifications of antennas, are all comparatively significant. The effectiveness of these systems is heavily influenced by the design and placement of antennas, as improper installation or positioning often leads to poor performance [3].

In modern microwave and wireless engineering, the growing demand for compact antenna systems has made antenna miniaturization become a significant research focus. Among the various antenna structures, microstrip patch antennas (MPAs) have gained a lot of attention because of their compact profile. In fact, MPA also considered as the modest form of the antenna arrangement which used the microstrip technique for fabrication purpose to keep the antenna size small and can be simply mounted on a circuit board [4]. Despite its compact size, MPA also offered distinct characteristics such as, low cost, light weight, low profile and patching in various geometric shapes.[5].

The strong and growing demand for antennas that can operate efficiently at high frequencies is driven by the need for higher data rates, wider bandwidth, and improved resolution in modern systems, and this demand has been increasing across several fields, including satellite systems, radar systems and Internet of Things (IoT). However, there are still a great deal of problems and limitations that must be dealt with; the narrow bandwidth and the efficiency of the radiation will be poor due to the small size of the antenna, leading to degradation in antenna performance. In the early development of antennas, metal was chosen as a radiating element because of its high conductivity and to maximise the radiation efficiency. While traditional materials offer stability, they may face limitations. Their inherently narrow frequency bandwidth makes them only effectively operate within a limited range of frequencies [6]. Besides, due to the intrinsic characteristics of metal, the traditional metal-based antennas are corroded easily, causing economic losses and degrading performance and lifespan. Several methods have been employed such as radome, sacrificial anodes protection and alloys with corrosion-resistance in order to reduce the corrosion of antenna. However, these approaches are often costly to implement and reduce metal conductivity, hence negatively impacting radiation efficiency [7].

Thus,it was necessary to investigate radiating patch materials with improved performance characteristics. To address these limitations, ferrite-based MPA is proposed as an alternative to the conventional metallic layer in the antenna patch. The study analyzes how Mg substitution in nickel zinc ferrite modifies the structural and magnetic properties of the material and evaluates the resulting impact on impedance matching and bandwidth enhancement in MPAs. The MPA design was developed for X-band applications due to this frequency range is relevant especially for satellite communication, Internet of Things (IoT) systems, and defense radar, where compact size, stable radiation characteristics, and reliable high-frequency performance are essential.

2.0 THEORY/LITERATURE REVIEW

Ferrite-based materials provide a low cost and stable alternative for patch fabrication [8].Spinel-type ferrite has increased tremendous interest among researchers due to its excellent magnetic and dielectric performance, along with its physical and chemical stability. Within the subclass of ferrites, Ni–Zn ferrites are considered the most adaptable ferrites as a result of their novel characteristics that make them ideal for high-frequency applications [9]. Ni-Zn ferrites are widely utilized as core materials in numerous electromagnetic devices and extensive industrial applications, including inductors, microwave components, power supplies, transformers for both high and low frequencies and antenna rods [10]. These wide range of applications are owing to their high saturation magnetization, high magnetic permeability, good chemical stability, exceptional mechanical strength, high curie temperature (570 °C) and low losses [11]. Moreover, the high resistivity (10^6 Ω cm) of Ni-Zn ferrite make them a good candidate to be used in high frequency antennas in order to minimal the eddy current losses [12]. Beyond its excellent properties, Ni-Zn ferrites also offer great potential for enhancement due to their adaptable valence state, distinctive electronic configuration, and flexible structure, hence providing numerous opportunities for improvement [13]. Zhang [14] reported the $MgZnFe_2O_4$ have large magnetization values compared to $ZnFe_2O_4$, which basically approaches zero. Navneet *et al*. [15] discussed the magnetic moment measurements due to the incorporation of Mg in Ni–Zn spinel ferrites. The saturation magnetization first increases and then decreases with an increase in the concentration of Mg^{2+} ions. The values of coercivity decrease with an increase in Mg^{2+} concentration. With this motivation, it is expected that an appropriate amount of Mg^{2+} substitution can modify the overall ferrite structure, enhancing the permeability and magnetization of the sample, thereby achieving better impedance matching. Improved impedance matching will lead to superior antenna performance by reducing return loss, allowing the antenna to transmit signals more efficiently and at maximum strength.

3.0 MATERIALS

For the synthesis; Iron (III) oxide (Fe_2O_3) (96 %), Nickel (II) oxide (NiO) (99 %), Zinc oxide (ZnO) (99 %), Magnesium oxide (MgO) (99 %), α-terpineol (90 %), m-xylene (99 %) and linseed oil were procured from Sigma-Aldrich. All the chemicals and materials were used without further purification.

4.0 EXPERIMENTAL

4.1 Synthesis of Mg-NZF

Ferrite powders Mg-NZF, with the general formula $Ni_{0.3}Zn_{0.7-x}Mg_xFe_2O_4$ ($x = 0.0, 0.2, 0.4$ and 0.6) were synthesized using the mechanochemical technique [16]. Stoichiometric quantities of iron oxide, nickel oxide, zinc oxide and magnesium oxide that have been calculated with mol percentages were milled for 6 hours using a Cole-Palmer BM-450 SPEX equipped with a hardened steel vials and balls. The steel vial and grinding balls were used, and the ball-to-powder weights ratio of (BPR) 10:1. The milling was performed at 1450 rotation per minute (rpm) at room temperature in a deionized water medium. The obtained mixture was dried in the oven at 80 °C for 12 hours and then calcined at 800 °C for 2 hours in an air atmosphere. The calcined powders were milled again at 1450 rpm rotation speed for a milling time of 1 hour. The dry powders were granulated with 2 wt% PVA (Polyvinyl Alcohol) binder and pressed into toroidal shaped at a pressure of 5 tonnes. Subsequently, samples in powder and toroidal forms were underwent the conventional final-stage sintering process at 1200 °C for a duration of 8 hours in air, with a heating rate of 4 °C per minute.

4.2 Fabrication of Mg-NZF based patch antenna

The basic configuration of MPA generally consist of ground plane, dielectric substrate, radiating patch and feeding part. The ground plane is the lowest layer is often made of material that conducts electricity, whereas the substrate which is intermediate layer is most commonly from the material which has dielectric constant ε_r in the range of 2.2 to 12. The radiating patch is positioned on the top layer in antenna configuration and a microstrip feedline is positioned centrally along the width of the rectangular patch and etched on the same substrate layer. The patch antenna is wider than the feed line. The feed dimensions are selected to provide an impedance close to 50 ohms, which enables impedance matching between the feed and the patch antenna. [17]. With proper matching, energy is coupled more efficiently to the patch, resulting in better antenna performance. MPA was fabricated using a screen-printing technique. The screen printing technique was chosen over 3D printing because it is low cost, high material utilization and suitability for large area mass production [18]. This technique offers ease of operation and provides superior compatibility that can be used for large scale production on different substrates, including fabrics and polymers [19]. The organic binder was firstly prepared by mixing 85.0 wt% linseed oil with 12.5 wt% m-xylene using magnetic stirrer at 250 rpm for 3 hours. Then, 2.5 wt% α-terpineol was added to the mix and then continued stirring for another 2 hours [20]. The prepared binder was added to the sample powder with different powder to binder weight ratios and mixed using a vortex mixer for 30 minutes to obtain a homogenous paste for thick film printing. The FR4 substrate was selected due to its low cost [21] and high mechanical strength [22]. The prepared thick film paste was printed screen printed onto the FR4 substrate using a silk-screen frame and squeegee, then underwent dried and fired at 200 °C for 30 minutes to ensure adhesion of the thick film paste onto the substrate. A subMiniature connector is then adhered to the patch antenna by using silver paste and copper tape for further measurement. The schematic diagram of the fabricated MPA and its specifications are given in Fig. 1 and Table 1, respectively.

4.3 Characterization

The structure of the sintered sample was measured by using Rigaku Miniflex II X-ray Diffractometer. Images of their microstructure were obtained using a scanning electron microscope (SEM, JEOL JSM-IT200). The Fourier transmission infrared (FTIR) measurements in the studied samples were carried out (contained within a KBr matrix) by Perkin Elmer Spectrum 100 Spectrometer in a region of wave number from 400–4000 cm^{-1} to determine the functional groups and bonds in all materials. Magnetic hysteresis loops were measured by using a vibrating sample magnetometer (VSM, Lake Shore 7410). The performances of the microstrip patch antenna were measured with return loss analysis using PNA N5227A Vector Network Analyzer.

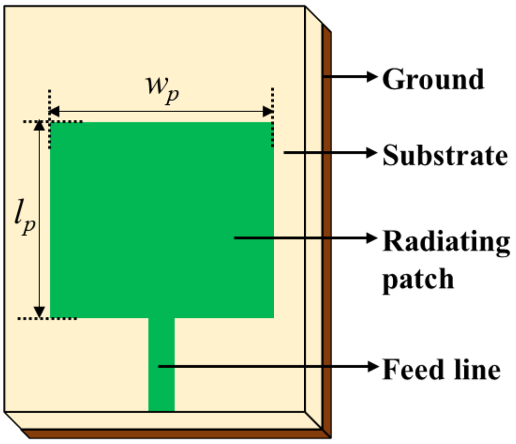

Fig. 1 Configuration of a rectangular MPA.

TABLE 1: Specifications of patch antenna

Parameter	Value
Dielectric constant, ε_r	4.3
Substrate thickness, h	1.6 mm
Patch width, w_p	15 mm
Patch length, l_p	11 mm

5.0 RESULTS AND DISCUSSION

5.1 XRD Analysis

Fig.2 shows the multi-plot of X-ray diffraction spectra of the sintered $Ni_{0.3}Zn_{0.7-x}Mg_xFe_2O_4$ (x = 0.0, 0.2, 0.4 and 0.6) samples at 1200 °C. The diffraction patterns are listed to (220), (311), (222), (400), (422), (333), (440), (620), (533) and (622) reflection planes, accordingly at 2θ values of 30.06°, 35.40°, 37.03°, 43.022°, 53.37°, 56.97°, 62.56°, 70.98°, 74.01° and 75.02°. The diffraction peaks found are notable because they closely corresponding to the standard crystallographic phase as mentioned in reference code 98-006-8765 and also to those found in earlier research on spinel ferrites [21, 22]. The most intense (311) plane confirms the formation of a single-phase face centred cubic spinel. The samples do not exhibit any significant changes in peak position or additional impurity phase, which suggests that the Mg^{2+} is completely incorporated in the host nickel zinc ferrite lattice [25]. The *d* spacing, lattice constant and unit cell volume were calculated using the most prominent peaks (311) in each sample, as shown in Table 2. The lattice constant, *a* was determined via the following formula [26]:

$$a = d\sqrt{h^2 + k^2 + l^2} \tag{1}$$

where *d* is the interplanar spacing and *hkl* are the Miller indices of the lattice planes. The lattice constant for the (311) peaks of Mg-substituted NiZn ferrites as shown in Table 1, initially increased from 8.3891 Å to 8.3950 Å at (x = 0.2), then decrease in value of lattice parameters 8.3818 Å at (x = 0.4) and later increased to 8.4010 at (x =0.6) with increased concentration of Mg. The resultant variation in lattice parameter does not appear to be a simple linear function. Based on the fact that the radius of Mg^{2+} ions (0.72 Å) has a smaller ionic radius compared to that of Zn^{2+} ions (0.74 Å). The lattice parameter was expected to decrease with increasing magnesium substitution, following Vegard's law However, deviations from Vegard's law may occur due to the preferential occupation of Mg^{2+} ions at both tetrahedral and octahedral sites, which modifies the local lattice strain [27].

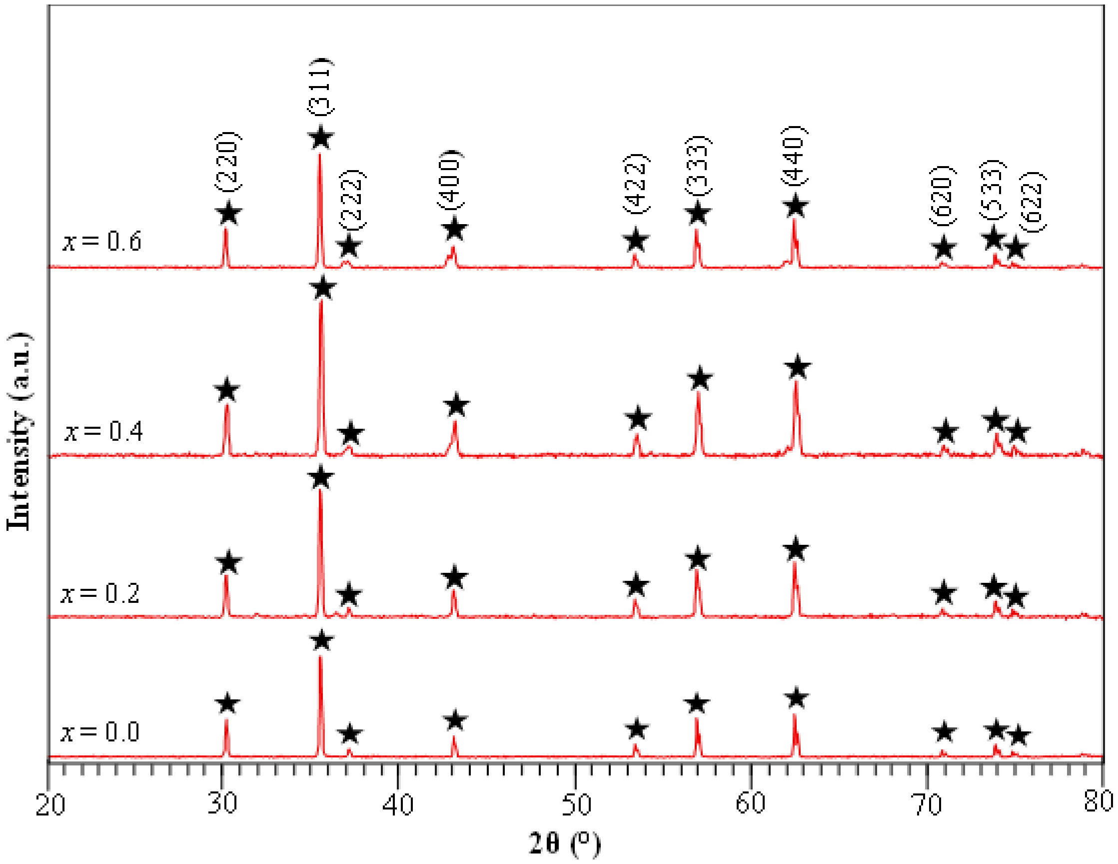

Fig.2: X-ray diffraction patterns for $Ni_{0.3}Zn_{0.7-x}Mg_xFe_2O_4$ (x = 0.0 to 0.6).

TABLE 2: Structural parameters based on XRD spectra for Mg substituted NZF

Mg concentration, *x*	Peak position (°)	Most intense phase	Space group	(hkl)	d-spacing	a (Å)
0.0	35.4915	$NiZnFe_2O_4$	Fd3m	311	2.52938	8.3891
0.2	35.4658	$MgNiZnFe_2O_4$	Fd3m	311	2.53115	8.3950
0.4	35.5228	$MgNiZnFe_2O_4$	Fd3m	311	2.52722	8.3818
0.6	35.4388	$MgNiZnFe_2O_4$	Fd3m	311	2.53302	8.4010

Vegard's law However, deviations from Vegard's law may occur due to the preferential occupation of Mg^{2+} ions at both tetrahedral and octahedral sites, which modifies the local lattice strain [27].

5.2 SEM Analysis

Scanning electron microscopy (SEM) was utilized to examine the microstructure and morphology of ferrites. Fig. 3 shows SEM image captured at 7000 x magnification with a 2 µm observation range, alongside histograms illustrating the particle size distribution. The magnesium concentration in Ni-Zn ferrites was found to significantly affect the particle size and structural shape. From the micrographs, it is obvious that the samples exhibit mostly polygonal shapes with flat and faceted faces. There are no obvious large pores or necks between grains, indicating sintering has progressed beyond initial neck formation and particle rearrangement. The microstructure seems uniform and dense, typical of a material after high temperature sintering where grain growth and densification are dominant. Moreover, the randomly selected 200 particles from the SEM images were represented as whole particles to measure the particle size distributions by using a J-image software. The effect of Mg^{2+} ion towards the particle size distribution can be observed in histograms in Fig 3. The average particle sizes of samples of obtained have ranges between 2.33 µm to 3.33 µm as Mg content increased from x = 0.0 to 0.4. As reported by [28], Mg acts as a sintering aid by promoting grain growth and enhancing densification. This aligns with the observed increase in particle size with higher Mg content and the microstructural evolution in the samples.

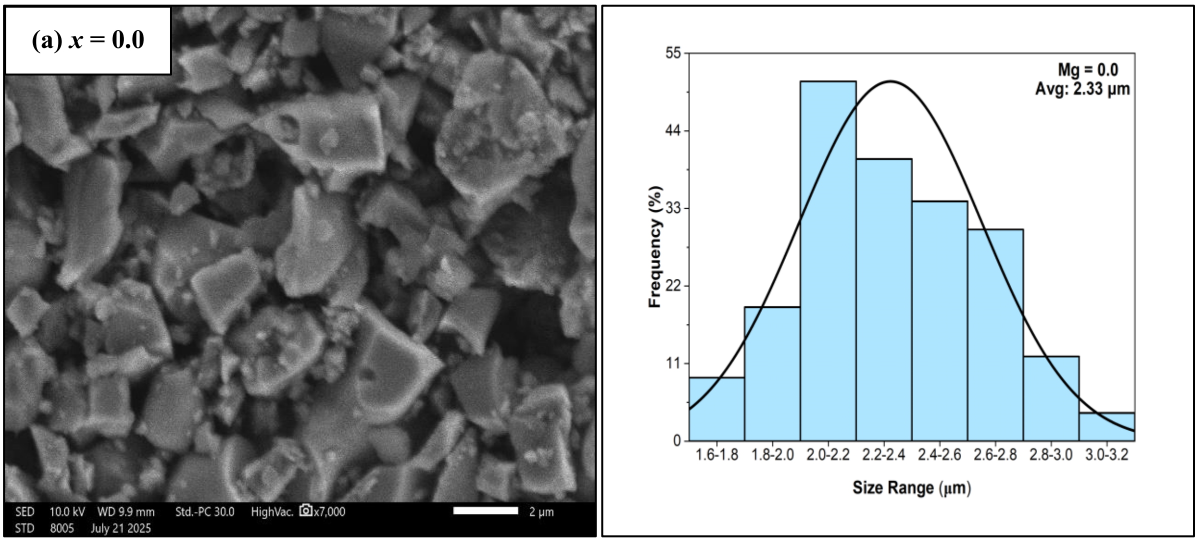

Fig.3: Continued

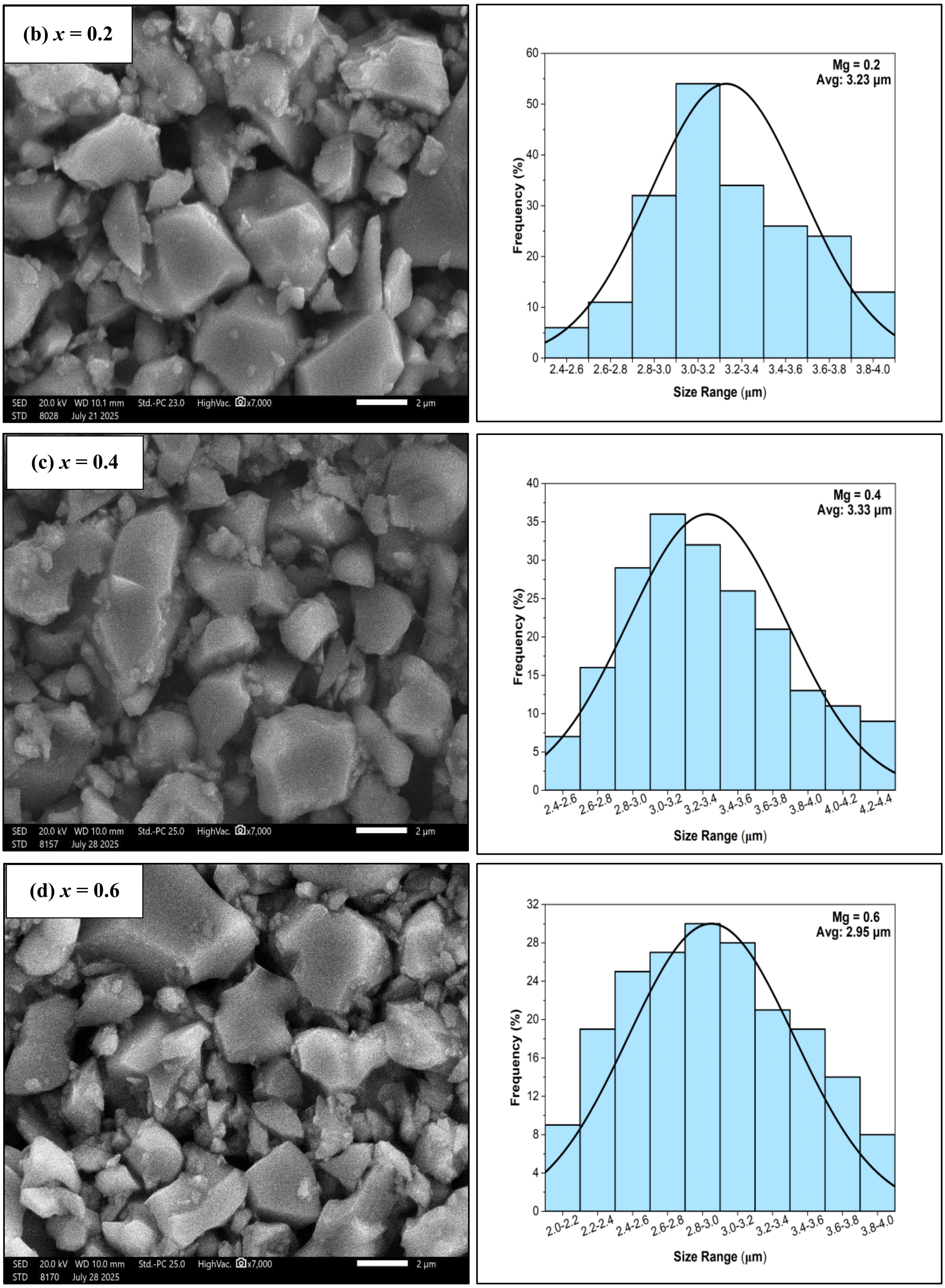

Fig.3: SEM micrographs under magnification of 7000× with corresponding histograms of particle size distribution of $Ni_{0.3}Zn_{0.7-x}Mg_xFe_2O_4$ samples sintered at 1200 °C.

5.3 FTIR Analysis

The analysis of chemical bonding of the sintered $Ni_{0.3}Zn_{0.7-x}Mg_xFe_2O_4$ samples has been carried out by using Fourier transform infrared spectroscopy (FTIR) [29]. Fig 4. shows the spectrum measured in the region of 4000-400 cm^{-1}. The FTIR spectra of all examined powder series exhibit two prominent absorption bands, v_1 (about 570 cm^{-1}) and v_2 (about 429 cm^{-1}) in the range of 400-600 cm^{-1}. These two absorption bands are defined as [23]:

$$v = \frac{1}{2\pi c}\sqrt{\frac{k}{\mu}} \qquad (2)$$

where v is the wavenumber, c is the speed of light, k is the force constant and μ represents the reduced mass of ions. The observed absorption band reveals the formation of a single phase spinel structure [30]. The absorption band at 569.42 cm^{-1} and 425.66 cm^{-1} is attributed to the intrinsic stretching vibration of Fe^{3+}–O^{2-} in tetrahedral and octahedral site respectively [31]. The v_2 band shifts shifts towards higher wavenumber side with increasing Mg^{2+} content, indicating reduced Fe-O bond length due to site substitution. This can be attributed to the fact that Mg^{2+} ions might be occupying the octahedral sites. As Mg^{2+} ions (0.72Å) have a larger ionic radius than Fe^{3+} ions (0.55Å), they push the Fe^{3+} ions towards oxygen ion resulting in decreased Fe^{3+}-O^{2-} bond length. Hence, the shorter the bond length corresponds to the stronger bond (larger k) which in turn may be responsible for the increase the fundamental frequency of vibration of the tetrahedral site [15]. In addition, an increase in force constants (k), reflects the stronger of bonding within the crystal lattice, particularly between the cations and oxygen ions [31]. The peaks present at 1380.53 cm^{-1} and 1622.66 cm^{-1} are attributed to carboxyl group (COO^-) and stretching of C-H bonds respectively. While the broad peaks at 3413.61 cm^{-1} were linked with stretching vibration of the O-H group in the samples [32].

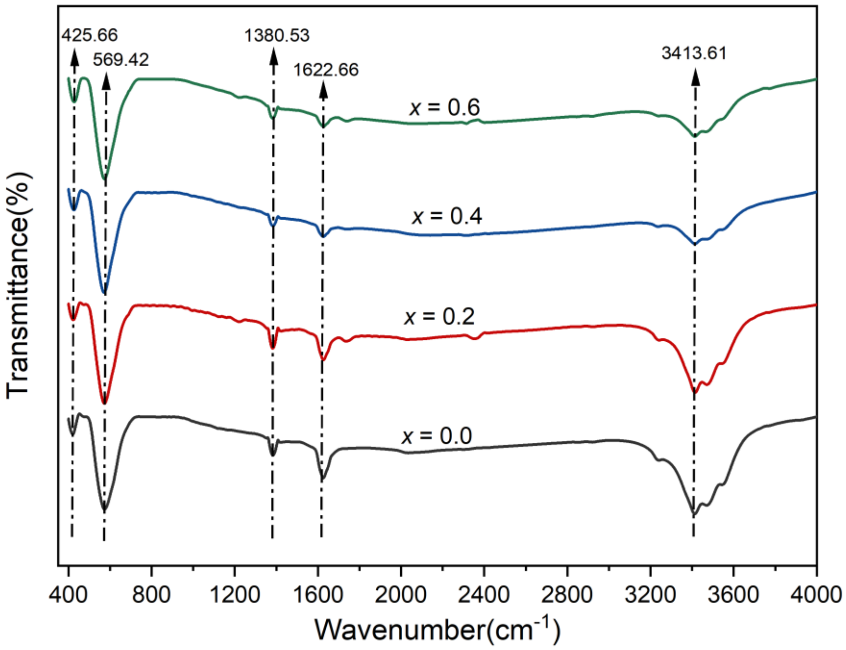

Fig 4: FTIR spectra of $Ni_{0.3}Zn_{0.7-x}Mg_xFe_2O_4$ (x = 0.0, 0.2, 0.4 and 0.6)

5.4 Magnetic Properties

The magnetic nature of the prepared Mg-NZF samples was analyzed using vibrating sample magnetometer (VSM) by applying a maximum magnetic field (±12 kOe) which indicates that the samples exhibited magnetic behavior. The room temperature of magnetization (M) versus magnetic field (H) curves (hysteresis loop) of prepared samples are displayed in Fig 5. The narrow breadth (S-shaped) of the hysteresis curve and small H_c values signify that this sample is a type of soft ferrite, which can be easily magnetized and demagnetized under low applied magnetic field [33]. Table 3 shows the quantitative results of saturation magnetization (M_s) and coercivity (H_c), which were determined to be in the range of (47.46–62.07) emu/g and (34.51–38.37) Oe respectively. Generally, magnetization increases as the applied magnetic field is raised, until it reaches a saturation point at higher fields where all magnetic moments are fully aligned. Beyond this saturation, increasing the magnetic field does not significantly increase the magnetization, as the material attains its maximum magnetic response. It was found that the saturation magnetization (M_s) increases up to 62.07 emu/g at a Mg concentration of $x = 0.4$. As the concentration is increased further to $x = 0.6$, the saturation magnetization value decreases to 54.32 emu/g. In Ni-Zn ferrites system, Zn^{2+} ions strongly prefer to occupy the tetrahedral (A) sites, while Ni^{2+} and Mg^{2+} ions mainly occupy the octahedral (B) sites. Fe^{3+} ions have an equal tendency to be distributed between both A and B sites. The saturation magnetization is influenced by the distribution of Fe^{3+} ions among the tetrahedral (A) and octahedral sites (B) [23]. By increasing the concentration of Mg^{2+} (0 μB) ions displace the Fe^{3+} (5 μB) ions from the A site to B site, eventually will enhances A-B super exchange effect and results in an increased value of M_s. Despite of cation distribution, the increased of grain size at $x = 0.4$ facilitated magnetic domain alignment, resulting in the highest magnetization (62.07 emu/g).

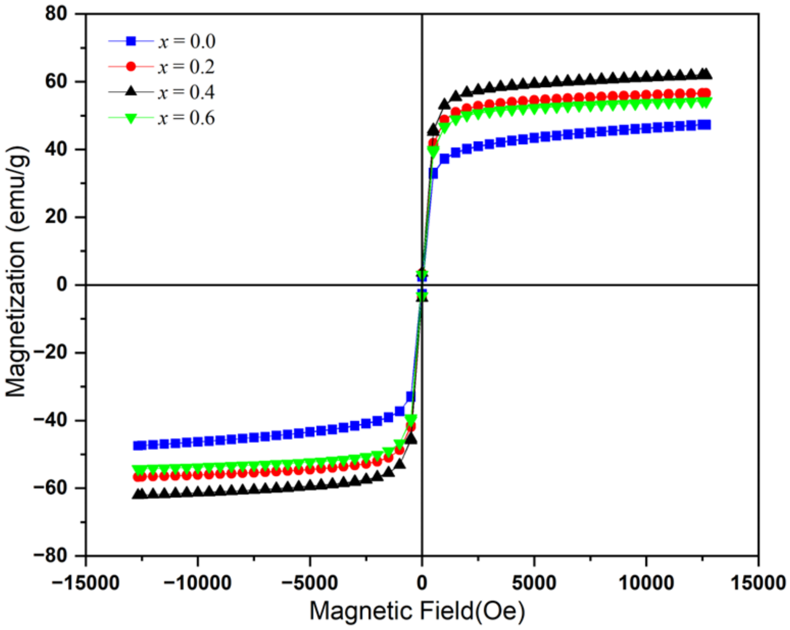

Fig 5: Magnetic hysteresis loop of $Ni_{0.3}Zn_{0.7-x}Mg_xFe_2O_4$ (x = 0.0, 0.2, 0.4 and 0.6)

TABLE 3: Variation of magnetic parameters with different Mg concentrations

Mg concentration, *x*	**Saturation Magnetization, M_s (emu/g)**	**Remanence Magnetization, M_r (emu/g)**	**Coercivity, H_c (Oe)**
0.0	47.46	2.43	34.51
0.2	56.70	3.44	38.37
0.4	62.07	3.73	38.06
0.6	54.32	3.18	37.42

5.5 Return Loss

The performance of an antenna depends on several performance metrics such as S-parameter (S_{11}) and bandwidth. The variations of return loss (RL) as a function of frequency of silver patch and Mg substituted NZF is depicted in Fig. 6. The values of RL at corresponding operating frequency and -10 dB bandwidth are tabulated in the Table 4. The RL indicates that how perform an antenna could transfer power from a source to the antenna [34]. From Fig. 6, it could be observed that, the silver sample exhibited a lowest negative return loss of -19.35 dB, indicating relatively poor impedance matching. Increasing concentration of magnesium from 0.0 to 0.4 significantly enhances the microwave absorption properties of the samples, which demonstrates a substantial increment of negative RL of the samples starting from -33.17 dB to -37.98 dB. It can be seen that each material has a strong ability to absorb microwaves. The antenna at $x = 0.4$ exhibits the highest negative return loss (-37.98 dB), which align with the output from SEM and saturation magnetization. The magnesium concentration in NZF was found to significantly influence the particle size and structural morphology. The increase in particle size may enhance the relative permeability, which in turn contributes to an increase in the net magnetic moment and consequently higher $M_{s.}$ This improvement facilitates better impedance matching between the patch and the feed line. As a result, more efficient power transfer is achieved, leading to the observed higher negative RL. The measured bandwidths for

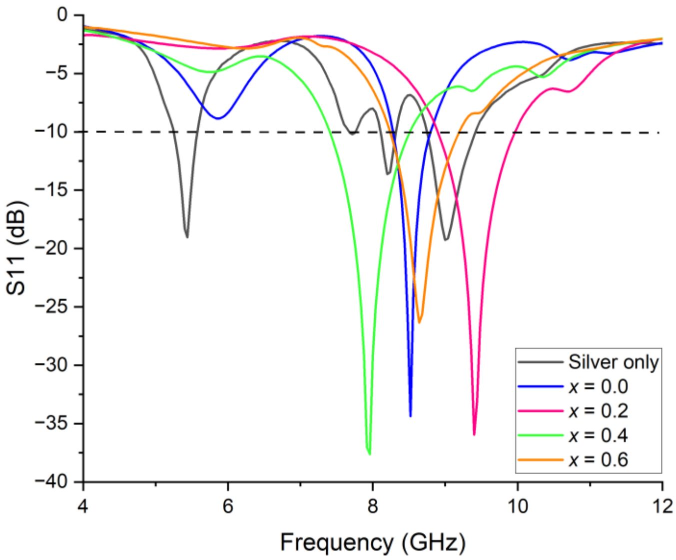

Fig 6: Return loss (S11) characteristics of $Ni_{0.3}Zn_{0.7-x}Mg_xFe_2O_4$ based MPAs; the –10 dB reference is shown by the dotted line

TABLE 4: Outcomes of the proposed MPA

Mg concentration, x	Frequency (GHz)	Return Loss (dB)	Effective Bandwidth at -10dB (GHz)
silver	9.02	-19.35	0.67
0.0	8.50	-33.17	0.49
0.2	9.42	-36.03	1.07
0.4	7.95	-37.98	1.12
0.6	8.65	-26.49	0.94

all samples are in the range of 0.49-1.12 GHz. The bandwidth was defined as the difference between the highest and lowest frequencies in a continuous band of frequencies. The bandwidth of the of Mg substituted NZF based patch antenna was measured at -10 dB, which meets the accepted antenna design standard as it indicates that the antenna reflects only 10% of the power while radiating at least 90% effectively [35]. The overall observations about the return loss and -10 dB % bandwidth, it is inferred that the x = 0.4 ferrite has potential to be used as a radiating patch for microstrip patch antenna.

6.0 CONCLUSION

This study concludes that magnesium substitute nickel zinc ferrite shows promising potential for developing microstrip patch antennas used in microwave antenna and wireless communication technologies. Conducting an in-depth investigation of Mg substituted NZF paste synthesized using the mechanochemical technique including examination of phase, functional groups, and morphology together with the magnetic nature of Mg substituted NZF shows the impact of substitution of magnesium in nickel zinc ferrite system. The optimal magnesium content at x = 0.4 resulted in a saturation magnetization of 62.07 emu/g, a return loss of –37.98 dB, and a bandwidth of 1.12 GHz, demonstrating a strong correlation between magnetic enhancement and antenna performance. These results highlight Mg substituted NZF as a potential ferrite material for improving patch antenna performance.

ACKNOWLEDGEMENTS

The authors gratefully acknowledge Universiti Malaysia Pahang Al-Sultan Abdullah (UMPSA) for their financial support under the Post-Graduate Research Scheme (PGRS230368). Appreciation is also extended to the Ministry of Higher Education for funding provided through the Fundamental Research Grant Scheme No. FRGS/1/2021/TK0/UMP/02/54 (University Reference RDU210152), which made this research possible.

REFERENCES

1. N. M. Sayem, A. K. M. Baki, F. Faysal, S. T. Mahmud, A. Jubayer, and T. A. Rifat, “Development of Novel and High Gain Microstrip Patch Antennas at Different Frequency Bands for 6G Applications,” Progress In Electromagnetics Research, vol. 137, pp. 263–275, 2023.
2. M. S. Rana et al., “At 28 GHz microstrip patch antenna for wireless applications: a review,” Telkomnika (Telecommunication Computing Electronics and Control, vol. 22, no. 2, pp. 251–262, 2024.
3. V K. Garg, “Chapter 10 Antennas, Diversity, and Link Analysis,” in Wireless Communications & Networking, pp. 287–316, 2007.
4. M. T. Islam et al., In: Proceedings of Second International Conference on Recent Advances in Materials and Manufacturing 2020, pp. 1502–1505.

5. S. K. Ezzulddin, S. O. Hasan, and M.M. Ameen, “Microstrip patch antenna design, simulation and fabrication for 5G applications,” Simul. Model. Pract. Theory, vol. 116, no. January, 2022.
6. S. Siragam, “Nanocomposite marvels: Miniaturized high bandwidth microstrip patch antenna for X-band applications,” Next Mater, vol. 5, no. July 2023, pp. 100243, 2024.
7. Y. Hui et al., “Graphene-Assembled Film-Based Reconfigurable Filtering Antenna with Enhanced Corrosion-Resistance,” Crystals, vol. 13, no. 5, 2023.
8. M. Zain Ul Abidin, M. Ikram, S. Moeen, G. Nazir, M. B. Kanoun, and S. Goumri-Said, “A comprehensive review on the synthesis of ferrite nanomaterials via bottom-up and top-down approaches advantages, disadvantages, characterizations and computational insights,” Coord. Chem. Rev, vol. 520, 2024.
9. Q. Yu, Y. Su, R. Tursun, and J. Zhang, “Synthesis and characterization of low density porous nickel zinc ferrites,” RSC Adv, vol. 9, no. 23, pp. 13173–13181, 2019.
10. H. Singh et al., “Ultrasonically assisted solvohydrothermal synthesis of nanocrystalline Zn-Ni ferrite advanced material for EMI shielding,” J. Alloys Compd, vol. 906, p. 164199, 2022.
11. R. Dosoudil, M. Soka, M. Usakova, E. Usak, V. Jancarik, and E. Dobrocka, “Magnetic and Structural Properties Analysis of Cerium Substituted Nickel-Zinc Ferrites,” IEEE Transactions on Magnetics, vol. 58, no. 2. 2022.
12. J. S. Ghodake, R. C. Kambale, T. J. Shinde, P. K. Maskar, and S. S. Suryavanshi, “Magnetic and microwave absorbing properties of Co^{2+} substituted nickel-zinc ferrites with the emphasis on initial permeability studies, ”Journal of Magnetism and Magnetic Materials, vol. 401, pp. 938–942, 2016.
13. S. F. Rafie, N. Abu-Zahra, and M. Sillanpää, “A comprehensive review of spinel ferrites and their magnetic composites as highly efficient adsorbents of rare earth elements,” Emerging Contaminants, vol. 11, no. 1, 2025.
14. Z. Zhang, “Study on the influence of magnesium doping on the magnetic properties of spinel Zn-Mg ferrite,” Materials Today Communications, vol. 26. 2021.
15. N. Singh, A. Agarwal, S. Sanghi, and P. Singh, “Effect of magnesium substitution on dielectric and magnetic properties of NiZn ferrite,” Phys. B Condens. Matter, vol. 406, no. 3, pp. 687–692, 2011.
16. M. Derakhshani, E. Taheri-Nassaj, M. Jazirehpour, and S. M. Masoudpanah, “Structural, magnetic, and gigahertz-range electromagnetic wave absorption properties of bulk Ni–Zn ferrite,” Sci. Rep, vol. 11, no. 1, pp. 1–13, 2021.
17. M. A. Saadi, E. Engineering, C. Seker, and E. Engineering, “Overview on Feeding Techniques of Microstrip Patch Antenna,” vol. 2, no. April, 2022.
18. S. H. Lin, C. Te Wu, Y. T. Yang, D. Z. Huang, J. Y. Wang, and J. J. Huang, “Design and fabrication of 5G silver thin film monopole antenna by screen printing process,” MRS Commun, vol. 15, no. 3, pp. 506–513, 2025.
19. K. Zhou, R. Ding, X. Ma, and Y. Lin, “Printable and flexible integrated sensing systems for wireless healthcare,” Nanoscale, vol. 16, no. 15, pp. 7264–7286, 2024.

20. I. H. Hasan et al., “Nickel zinc ferrite thick film with linseed oil as organic vehicle for microwave device applications,” Mater. Chem. Phys., vol. 236, no. April, 2019.
21. G. Srinivasu, T. Gayatri, D. M. K. Chaitanya, and V. K. Sharma, “Influence of FR4 material substrate on diamond slotted ultra wideband antenna in 1.71 GHz to 12 GHz,” Mater. Today Proc., vol. 45, pp. 5642–5648, 2021.
22. C. Balamurugan, T.S Arun Samuel, M. G. Raj S, P. Mary S, and S. Geege A, “Enhancing gain and bandwidth in a multiband microstrip patch antenna through L-slot and partial ground plane integration,” Scientific Reports, vol. 15, no. 1, pp. 2–13, 2025.
23. J. Zhao et al., “Influence of Mg^{2+} replacement on the structure and magnetic properties of $Mg_xZn_{1-x}Fe_2O_4$ ($x = 0.1–0.5$) ferrites,” J. Mater. Sci. Mater. Electron, vol. 32, no. 4, pp. 4008–4020, 2021.
24. N. Idayanti, Dedi, T. Kristiantoro, N. Sudrajat, D. Mulyadi, and A. Gustinova, “Effects of varying chemical composition with $x = 0.1$ - 0.7 on magnetic properties of soft ferrite $Ni_{1-x}Zn_xFe_2O_4$,” IOP Conf. Ser. Mater. Sci. Eng, vol. 620, no. 1, pp. 0–8, 2019.
25. S. Joshi, M. Kumar, S. Chhoker, A. Kumar, and M. Singh, “Effect of Gd^{3+} substitution on structural, magnetic, dielectric and optical properties of nanocrystalline $CoFe_2O_4$,” J. Magn. Magn. Mater, vol. 426, no. August 2016, pp. 252–263, 2017.
26. A. Sattar, B. Bofeng, M. Khalil, and M. Sajjad, “Detailed analysis of structural, optical and photo catalytic properties of spinel nickel doped magnesium zinc ferrites at different substitutions,” Inorg. Chem. Commun, vol. 142, no. May, 2022.
27. A. M. Mohammad, S. M. Ali Ridha, and T. H. Mubarak, “Structural and Magnetic Properties of Mg-CoFerrite Nanoparticles,” Digest Journal of Nanomaterials and Biostructures, vol. 13, no. 3, pp. 615–623, 2018.
28. S. Y. Lee, R. Nazlan, I. R. Ibrahim, and G. Bahmanrokh, “Influence of Mg and Ti substitutions on structural , microstructural, and magnetic characteristics of Ni-Zn ferrites,” E3S Web of Conferences 681, vol. 03005, pp. 1–13, 2025.
29. S. Yonatan Mulushoa and N. Murali, “Comparison of Structural, dielectric and magnetic investigation of Cr^{3+} substituted Mg-Cu, Mg-Zn, and Mg-Ni ferrites system,” Inorg. Chem. Commun, vol. 145, no. September, p. 110033, 2022.
30. O. H. Abd-Elkader, N. M. Deraz, and L. Aleya, “Effects of Zinc Substitution on the Microstructural and Magnetic Characteristics of Cubic Symmetry Nickel Ferrite System,” Symmetry (Basel), vol. 15, no. 5, 2023.
31. J. Mazurenko et al., “Magneto-structural properties of Mg-substituted copper ferrite nanoparticles,” Mater. Res. Express, vol. 11, no. 12, 2024.
32. A. Tariq et al., “Optimizing optical, dielectric, structural, and electrical properties in Cu-substituted Mg-Zn ferrite nanoparticles: Insights for sustainable energy and environmental solutions,” J. Alloys Compd, vol. 1037, no. April, p. 182252, 2025.
33. S. Hasan and B. Azhdar, “Synthesis of Nickel-Zinc Ferrite Nanoparticles by the Sol-Gel Auto-Combustion Method: Study of Crystal Structural, Cation Distribution, and Magnetic Properties,” Adv. Condens. Matter Phys, vol. 2022, 2022

34. M. D. Jahan, C. Das, and N. Sarker, “Design Analysis of a Micro-strip Patch Antenna for RFID, WiMAX and X-band Applications,”1st International Conference on Advances in Science, Engineering and Robotics Technology 2019, vol. 2019, no. Icasert, 2019.
35. M. A. Jusoh, N. I. E. Pamin, N. I. Z. Azman, R. Nazlan, and S. A. Harun, “Feasibility and performance of TiCN-based patch antennas for microwave antenna applications,” J. Mater. Sci. Mater. Electron, vol. 35, no. 22, pp. 1–11, 2024.